CORE
Metadata, citation and similar papers at core.ac.uk
Provided by NERC Open Research Archive

JOURNAL OF GEOPHYSICAL RESEARCH, VOL. 116, A03223, doi:10.1029/2010JA016068, 2011

Magnetosonic wave instability analysis for proton ring distributions observed by the LANL magnetospheric plasma analyzer

Lunjin Chen,[1] Richard M. Thorne,[1] Vania K. Jordanova,[2] Michelle F. Thomsen,[2] and Richard B. Horne[3]

Received 30 August 2010; revised 9 December 2010; accepted 27 December 2010; published 18 March 2011.

[1] Energetic proton (1–45 keV) distributions measured by the magnetospheric plasma analyzer detector on Los Alamos National Laboratory geosynchronous orbiting satellites are analyzed to study the characteristics of proton ring development during the 2001 April storm. Distinct proton rings are formed over a broad spatial region from noon to premidnight, associated with individual or multiple substorm injections on the nightside. On the basis of observed proton distributions, the convective growth rate of magnetosonic waves is calculated. We find that these proton ring distributions can provide a source of free energy for exciting magnetosonic waves, with convective growth rate mostly in the range 10^{-5}–10^{-6} m^{-1}, over a broad range of frequency from a few times Ω_{H^+} up to ~35 Ω_{H^+} and over a broad magnetic local time range from 1000 to 2200.

Citation: Chen, L., R. M. Thorne, V. K. Jordanova, M. F. Thomsen, and R. B. Horne (2011), Magnetosonic wave instability analysis for proton ring distributions observed by the LANL magnetospheric plasma analyzer, *J. Geophys. Res.*, *116*, A03223, doi:10.1029/2010JA016068.

1. Introduction

[2] Fast magnetosonic (MS) waves, also called equatorial noise, at frequencies from a few Hz to several hundreds of Hz, are primarily confined within ~10° from the geomagnetic equator [*Russell et al.*, 1970; *Gurnett*, 1976;*Olsen et al.*, 1987; *Kasahara et al.*, 1994; *Santolík et al.*, 2002; *Němec et al.*, 2005] both inside and outside the plasmapause. Early observational studies [e.g., *Perraut et al.*, 1982; *Gurnett*, 1976] demonstrated that MS waves occur as a series of narrow tones, spaced at multiples of the proton gyrofrequency up to the lower hybrid resonance frequency f_{LHR}. It has been suggested [*Curtis and Wu*, 1979; *Perraut et al.*, 1982; *Boardsen et al.*, 1992; *Horne et al.*, 2000] that such equatorial MS waves can be excited at very oblique wave normal angles by a natural instability associated with a ring distribution ($\partial f/\partial v_\perp > 0$) of energetic protons at energies of the order of 10 keV whenever the velocity corresponding to the peak phase space density exceeds the local Alfven speed. A survey [*Meredith et al.*, 2008] of wave and particle data from the Combined Release and Radiation Effects Satellite (CRRES) confirmed the role of proton rings as a potential source mechanism. Recently both particle-in-cell simulation (K. Liu et al., Excitation of Bernstein waves in the terrestrial magnetosphere: Particle-in-cell simulations, submitted to *Journal of Geophysical Research*, 2010) and linear dispersion theory [*Gary et al.*, 2010] have also verified excitation of fast magnetosonic waves (referred to as ion Bernstein waves) due to proton rings.

[3] Equatorial MS waves can also influence radiation belt dynamics during active periods, leading to local electron acceleration from ~10 keV up to a few MeV in the outer radiation belt [*Horne et al.*, 2007]. For the strongest MS waves, the acceleration time scale of 1–2 days via electron Landau resonance is comparable to that due to whistler mode chorus waves [e.g., *Horne et al.*, 2005; *Li et al.*, 2007]. Furthermore, owing to the equatorial spatial confinement, energetic electrons in the outer radiation belt can be subject to nonresonant transit time scattering, in addition to the Landau resonant scattering predicted by quasi-linear theory [*Bortnik and Thorne*, 2010].

[4] Recently, *Chen et al.* [2010b] performed a global analysis of the MS instability based on energetic proton phase space density simulated by coupling the Rice Convection Model (RCM) and the Ring Current–Atmospheric Interactions Model (RAM) during a geomagnetic storm [*Jordanova et al.*, 2010; *Chen et al.*, 2010a]. Their detailed theoretical analysis showed that the MS wave instability occurs when the local Alfven speed is comparable to the proton ring velocity. Furthermore, the unstable frequency band is modulated by the ratio of the ring velocity and the local Alfven speed. Here we examine the characteristics of proton ring development from an observational point of view, and perform a magnetosonic wave instability analysis based on proton rings observed by the magnetospheric

[1]Department of Atmospheric and Oceanic Sciences, University of California, Los Angeles, California, USA.
[2]Los Alamos National Laboratory, Los Alamos, New Mexico, USA.
[3]British Antarctic Survey, Natural Environment Research Council, Cambridge, UK.

Copyright 2011 by the American Geophysical Union.
0148-0227/11/2010JA016068

plasma analyzer (MPA) detector on a Los Almos National Laboratory (LANL) geosynchronous orbiting satellite. The particle observations from MPA detectors have been used in the past to predict where and when plasma wave instabilities occur, e.g., whistler instability based on anisotropic electron observations [*MacDonald et al.*, 2008] and electromagnetic ion cyclotron wave instability driven by anisotropic ions [*Blum et al.*, 2009]. For the magnetosonic wave instability, ion distributions along the direction perpendicular to the ambient magnetic field ($\partial f/\partial v_\perp$) are relevant. In section 2, the ion observational data set is presented. Proton ring development and magnetosonic wave instability are investigated in section 3. Finally, we summarize our principal conclusions.

2. Data Set

[5] Energetic protons with energy between a few eV to ~45 keV are continuously monitored by the MPA detector on board several geosynchronously orbiting LANL spacecraft [*Bame et al.*, 1993]. Data obtained over a 4 day interval, 20–23 April 2001 covering the April 2001 geomagnetic storm, have been selected for analysis. The full three-dimensional (40 energies × 24 azimuths × 6 polar angles) distribution is measured in the spacecraft-centered coordinate system with z axis pointing along the spin axis toward the Earth's center. Although there is no direct in situ magnetic field measurement, the direction of the magnetic field is derived from the symmetry axis of the observed charged particle distributions [*Thomsen et al.*, 1996]. The 3D distribution is reorganized onto a regular grid in pitch angle (PA) and gyrophase (AZ) with respect to the ambient magnetic field direction by the standard triangle interpolation, producing a new distribution $f(E, \mathrm{PA}, \mathrm{AZ})$ where E is energy. The phase space density (PSD) at fixed 90° pitch angle, $f_\perp$, is then obtained by averaging over AZ at each energy channel. The Alfven speed $V_A = B/(\mu_0 m_{H^+} N_e)^{1/2}$, where m_{H^+} is the proton mass and N_e the background electron density, is calculated by assuming that N_e can be approximated as the sum of the measured low-energy (< 100 eV) proton number density N_{lp} and high-energy (≥ 100 eV) proton number density N_{hp}, and that the ambient magnetic field strength B can be obtained from a combination of a dipole internal field model and the Tsyganenko 96 external field model [*Tsyganenko*, 1995, 1996], which is a data-based model calibrated by instantaneous values of solar wind dynamic pressure, *Dst*, and the Y and Z components of the interplanetary magnetic field. The instantaneous values of these parameters are obtained through the SPDF OMNIWeb Plus service.

[6] On the basis of the ion phase phase density measurement by LANL satellites, we perform an instability analysis in section 3 by calculating the local equatorial growth rate of magnetosonic waves. A limitation of using LANL satellite data in the present study is the lack of wave measurement, and thus no direct comparison can be made between the predicted growth rate and observed magnetosonic wave emission. Nonetheless, such a limitation is compensated by the broad local time coverage of ion distributions near the equator, which provides the characteristics of ion ring distributions and indicates the preferential local time region where magnetosonic waves can be excited.

3. Proton Rings and Instability Analysis for Magnetosonic Waves

[7] Following the theoretical analysis of *Chen et al.* [2010b], the convective growth rate (measured along the direction of the wave group velocity) of highly oblique magnetosonic waves (wave normal angle $\theta \sim 89.5°$) for wave frequencies at exact multiples of the proton gyrofrequency ($\omega = m_\omega \Omega_{H^+}$, where m_ω is a whole number), can be expressed as

$$k_i = \int_0^{+\infty} dv_\perp W_\perp \frac{\partial f}{\partial v_\perp}\bigg|_{v_\parallel = 0}. \tag{1}$$

[8] The weighting function $W_\perp$ is given as

$$\begin{aligned} W_\perp = {} & \frac{2\pi^2 e^2}{\epsilon_0 m_{H^+}} \frac{\mathbf{k}\cdot\hat{\mathbf{v}}_g}{8n^2(2A'n^2 - B')} \frac{1}{\omega|k_\parallel|} v_\perp^2 \\ & \cdot \Big[n^4 \sin^2\theta \cos^2\theta (J_{m_\omega+1} - J_{m_\omega-1})^2 + (n^2\sin^2\theta - P) \\ & \cdot [2(L - n^2)J_{m_\omega+1}^2 + 2(R - n^2)J_{m_\omega-1}^2 \\ & + n^2 \sin^2\theta (J_{m_\omega+1} - J_{m_\omega-1})^2] \Big], \end{aligned} \tag{2}$$

where J_{m_ω} is Bessel function of order m_ω with argument $x = k_\perp v_\perp/\Omega_{H+}$, n is the refractive index for MS waves, P, L, and R are standard Stix coefficients, $A' = S \sin^2\theta + P\cos^2\theta$, $B' = RL \sin^2\theta + PS(1 + \cos^2\theta)$, and $\mathbf{k}\cdot\hat{\mathbf{v}}_g$ denotes the projection of wave normal vector $\mathbf{k}$ along the group velocity $\mathbf{v}_g$. We also assume that the refractive index n for MS waves can be obtained through the cold plasma dispersion relation for an electron-proton plasma. This formulation is valid for small growth rate in plasmas where the cold plasma dominates over a dilute hot species. As shown by *Chen et al.* [2010b] (Appendix B), the $v_\perp$ dependence of $W_\perp$ is of the form $J_{m_\omega}^2(k_\perp v_\perp/\Omega_{H+})$ for large m_ω (≥5), with aid of the following approximations: $\sin^2\theta \gg \cos^2\theta$, $L \approx -R$, and $n^2 \approx RL/S$.

[9] Figure 1 illustrates the type of ion distribution $f_\perp$ (thin solid line) that can give rise to magnetosonic waves. It features a secondary peak at $v_\perp = V_R$ (called the ring velocity) separated by a minimum at $v_\perp = V_{\mathrm{dip}}$ (called the dip velocity) from the main peak of low energies. In this diagram $V_{\mathrm{dip}} < V_A < V_R$ and positive gradients ($\partial f/\partial v_\perp$) only exist for $V_{\mathrm{dip}} < v_\perp < V_R$. The properties of $W_\perp$ and the gradients ($\partial f/\partial v_\perp$) determine the conditions under which MS wave instability can occur for such distributions. *Chen et al.* [2010b] have demonstrated that the velocity $v_{\perp\mathrm{peak}}$ of the peak in $W_\perp$ at fixed m_ω is typically in the vicinity of the Alfven speed (V_A) for small m_ω and drops as m_ω increases (schematically shown by the thick solid line in Figure 1). The frequency range of the MS instability (indicated by circles) may be approximately estimated as the frequency range over which $v_{\perp\mathrm{peak}}$ lies in the range (V_{dip}, V_R), namely where the $df_\perp/dv_\perp$ is positive. Waves with frequencies below (or above) this unstable frequency band are pre-

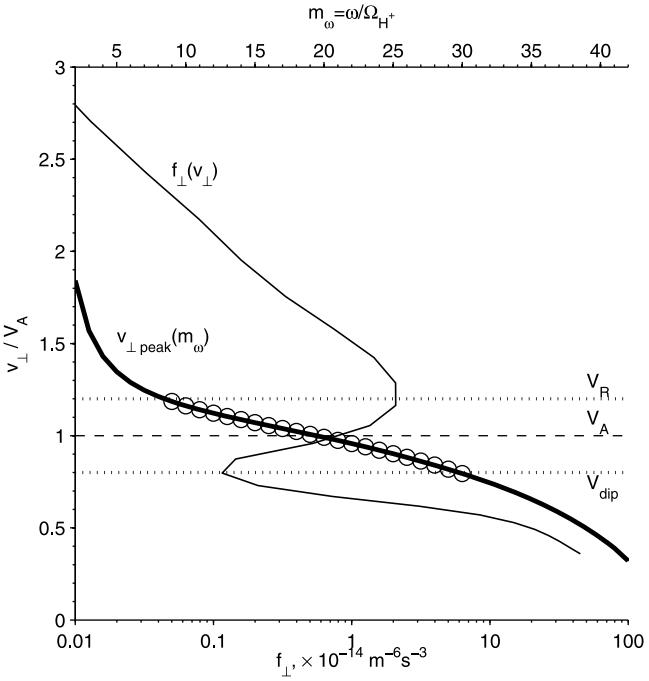

Figure 1. Schematic diagram to estimate the unstable frequency band of MS waves due to a proton ring distribution. The PSD of a proton ring along $v_{\|} = 0$, $f_{\perp}$ is plotted as the thin solid line as a function of $v_{\perp}$ normalized to the Alfven speed V_A (horizontal dashed line), with the top and bottom horizontal dotted lines for the ring velocity V_R and $V_{\rm dip}$, respectively. The $v_{\perp \rm peak}$ as a function of m_{ω} (= ω/Ω_{H^+}) is shown as the thick solid line. The frequency range of instability is indicated by the circles.

dominately damped by the negative gradients $df_{\perp}/dv_{\perp}$ associated with protons above V_R (or below $V_{\rm dip}$).

[10] Applying equation (1) to the observed data, we replace the velocity integral with a sum over the MPA energy channels:

$$k_i = \sum_j \int_{v_j}^{v_{j+1}} dv_{\perp} W_{\perp} \frac{\partial f}{\partial v_{\perp}}\bigg|_{v_{\|}=0} = \sum_j k_i^j, \qquad (3)$$

where j is the energy channel number, and k_i^j is the contribution due to the proton phase space density between energy channel j and $j + 1$. The energy interval corresponding to maximum contribution (maximum k_i^j) is identified as $E_{\rm dom}$. Because of the small average MPA count rates (<~5 counts per accumulation time of 9 ms) over the energy range 0.1–1 keV, only energy channels above 1 keV are used in this analysis to avoid statistical uncertainty in the measured gradients. The data fall into two categories: (1) cold plasma domination regime ($N_{\rm lp} > N_{\rm hp}$) and (2) hot plasma domination regime ($N_{\rm lp} \le N_{\rm hp}$). The calculation of the wave growth rate is limited to the cold plasma domination regime, where the formulations (1) and (3) are valid.

[11] An example of magnetosonic wave instability analysis is illustrated in Figure 2. Figure 2a shows the 2D PSD, averaged over the gyrophase, measured by the MPA detector on board the LANL-A01 spacecraft at 2001 UT on 20 April 2001 (magnetic local time 2035). The PSD $f_{\perp}$ along the $v_{\perp}$ axis, shown in Figure 2b, indicates a pronounced dip at $V_{\rm dip} \sim 0.9 \times 10^6$ ms^{-1} and a pronounced peak at $V_R \sim 1.1 \times 10^6$ ms^{-1}, comparable to the value of Alfven speed V_A ($\sim 1.2 \times 10^6$ ms^{-1}), which is obtained by assuming single-ion (H^+) plasma. Positive $df_{\perp}/dv_{\perp}$ in the $v_{\perp}$ range $V_{\rm dip} < v_{\perp} < V_R$ gives rise to unstable magnetosonic waves over the frequency range from 21 to 31 Ω_{H+}, with peak growth rate at 25 Ω_{H+}, as shown by blue circles in Figure 2c or Figure 2d. The wave frequency of the peak growth rate is consistent with the empirical relation (the heavy solid line in Figure 1) between the ratio V_R/V_A and wave frequency of peak growth rate: the value $V_R/V_A \sim 0.9$ corresponds to peak growth rate at frequency $\omega = 25\ \Omega_{H+}$. Wave damping at $\omega < 21\ \Omega_{H+}$ and $\omega > 31\ \Omega_{H+}$ is predominately due to negative $df_{\perp}/dv_{\perp}$ above the V_R and below the $V_{\rm dip}$, respectively.

[12] The measurement of total plasma density ($N_{\rm lp} + N_{\rm hp}$) from MPA detectors on LANL spacecraft is subject to error, primarily associated with high sensitivity of derived low-energy density ($N_{\rm lp}$) to uncertainties in the surface potential of the spacecraft. The absolute measurement of total density is estimated to be low by a factor of ~1.5–2 [*Denton et al.*, 2011], depending on the satellites (a factor of ~1.6 for the spacecraft LANL-01A). The effect of uncertainty of plasma density measurement is investigated by varying measured plasma density and shown in Figure 2c. The growth rate is calculated for both decreasing N_e by 50% (red pluses) and increasing N_e by 50% (green asterisks) and by 100% (magenta squares). As plasma density increases (or decreases) and thus V_R/V_A increases, the unstable frequency band shifts toward lower (or higher) frequencies, as expected from the empirical relation mentioned above. In this case 50% variation in plasma density results in a change of peak wave frequency by ~10 Ω_{H+}, and increase in plasma density by a factor of 2 leads to MS wave instability only below 7 Ω_{H+} and a decrease in the growth rate by a factor of ~3. Further increase in plasma density by a factor of >2.2 will result in suppression of wave growth at all the harmonic frequencies (not shown here). Therefore, the accuracy of plasma density measurement is important for predicting wave growth rate at each of the proton harmonic frequencies.

[13] No mass discrimination is made from the MPA measurement. Previous observations [e.g., *Young et al.*, 1982; *Roberts et al.*, 1987] have suggested that O^+ ions are present in the magnetosphere, especially during storm times. A recent statistical study [*Denton et al.*, 2011] shows a solar cycle dependence of the O^+ composition in the bulk plasma at geosynchronous orbit: from a typical value of ~20% at solar maximum to a low value ~0.2% at solar minimum. To investigate the effect of O^+ concentration, MS wave growth rate is also calculated with O^+ concentration η_{O+} = 10% and 20%, compared with that without O^+ ions, shown in Figure 2d. As the O^+ concentration increases and thus V_A decreases, the peak frequency of MS waves shifts slightly toward lower frequencies (22 Ω_{H+} for η_{O+} = 10% and 18 Ω_{H+} for η_{O+} = 20%), compared with 25 Ω_{H+} for η_{O+} = 0%.

[14] The above instability analysis for MPA measurement illustrated at a single time interval is used to perform a survey of MS wave instability over the 4 day period from

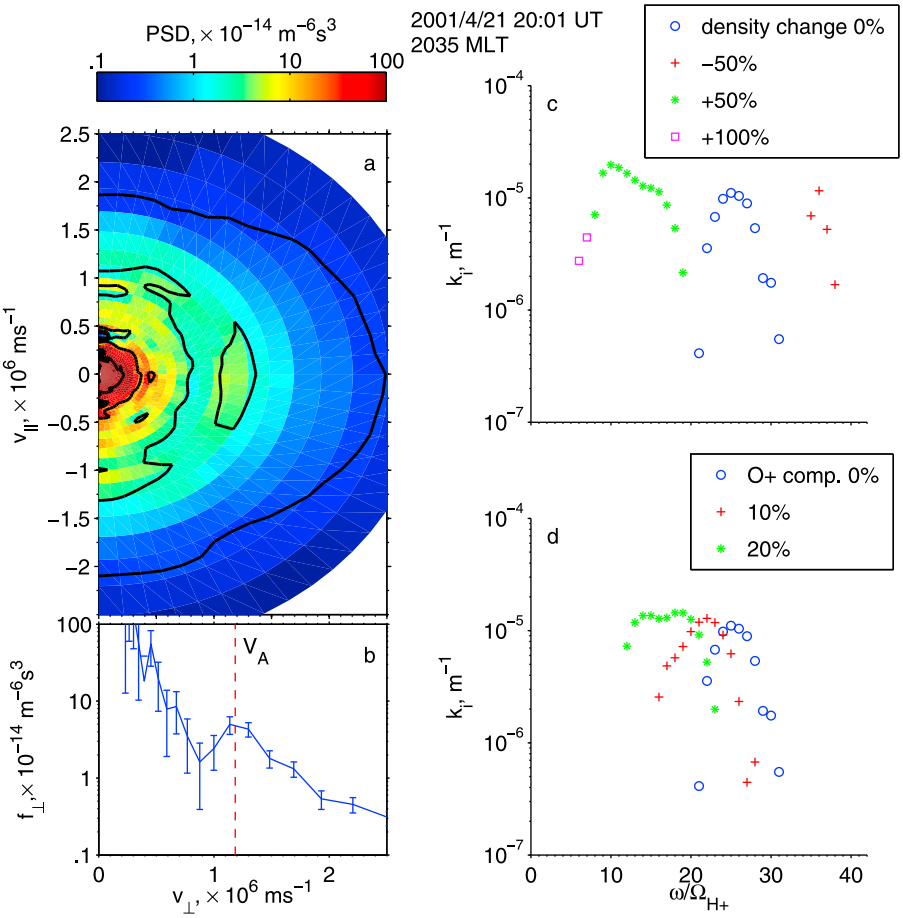

Figure 2. (a) Proton phase space density distribution measured at 2001 UT on 20 April 2001 by the MPA detector on board the LANL-A01 spacecraft. Solid lines represent PSD contours of value $10^{-15.5}$, $10^{-14.5}$, $10^{-13.5}$, and $10^{-12.5}$ m^{-6} s^3. (b) Proton phase space density along the $v_\perp$ axis, $f_\perp$, as a function of $v_\perp$. The uncertainty of PSD measurement is indicated by the error bars. The vertical dashed line represents the value of Alfven speed V_A on the basis of the measured ion density and assuming that H^+ is the only ion species. (c) The calculated convective growth rate k_i of magnetosonic waves based on measured ion phase space density (Figure 2b), as a function of wave frequency normalized to local proton gyrofrequency ω/Ω_{H^+}. The calculations are performed with varying ion density from the nominal value (0%) by −50%, +50%, and +100%, all with O^+ ion concentration $\eta_{O^+} = 0\%$. (d) Same as Figure 2c except that calculation is done with measured ion density and varying O^+ ion concentrations 0%, 10%, and 20%.

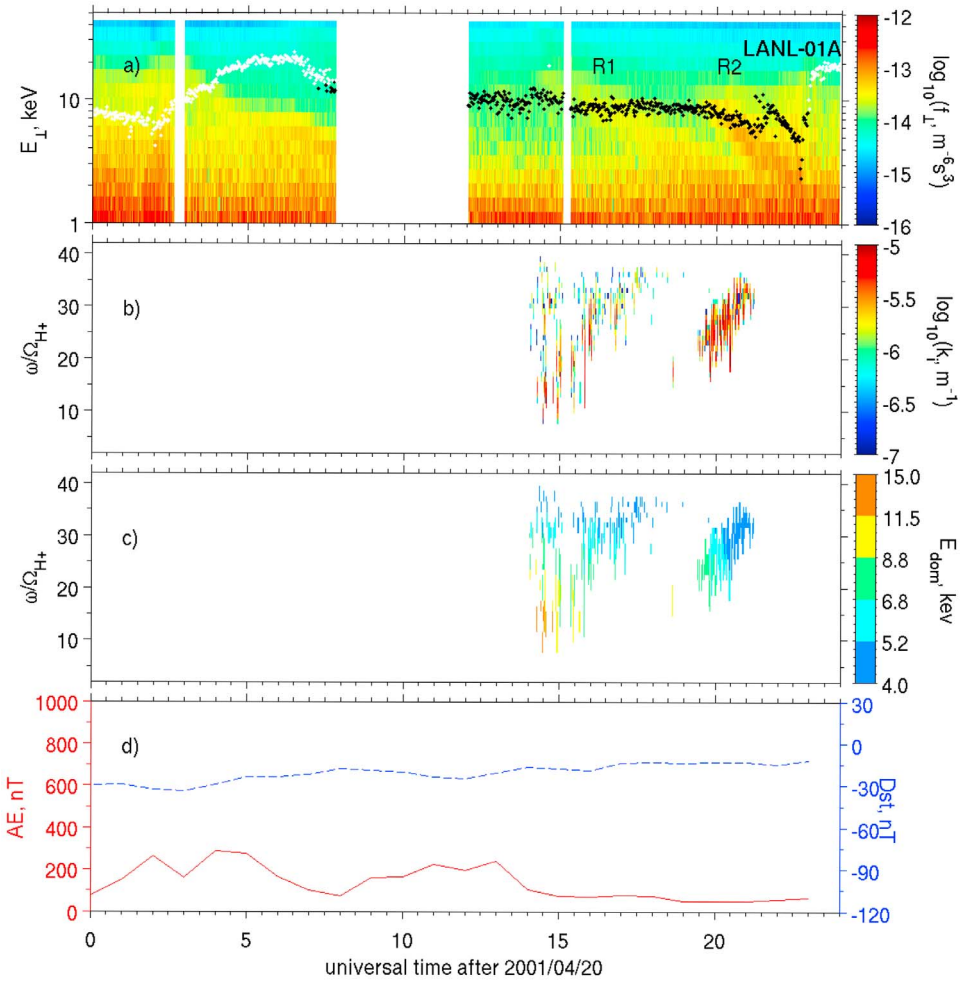

Figure 3. (a) The phase space density at pitch angle 90°, $f_{\perp}$, observed by the MPA detector on LANL-01A for 20 April 2001. The blank region is a data gap. The Alfven energy E_A is superimposed with dots, with white and black representing conditions $N_{lp} \leq N_{hp}$ and $N_{lp} > N_{hp}$, respectively. (b) Positive convective growth rate of magnetosonic waves in regions where $N_{lp} > N_{hp}$. (c) The energy interval contributing most to the magnetosonic wave growth rate shown in Figure 3b. (d) The geomagnetic indices *AE* (solid line) and *Dst* (dashed line). Note that MLT = UT + 0.55 h.

20 to 23 April 2001 during the 22 April 2001 storm. The calculation of the growth rate for the rest of paper is carried out by assuming that the plasma consists of only electrons and protons and that plasma density is accurately measured. Those two assumptions are still reasonable for the following two reasons. First, as shown in Figure 2d, large O^+ concentration (20%) only results in a slight shift of peak wave frequency by approximately a few Ω_{H+}, with peak growth rate about the same as that without O^+ ions. Secondly, although MS wave growth rate is sensitive to the plasma density, uncertainty of plasma density due to statistically fluctuations is compensated by the large number of cases studied.

[15] The observed proton phase space density at 90° pitch angle, $f_{\perp}(E_{\perp})$, on 20 April 2001 is shown in Figure 3a. Magnetic local time (MLT) follows the simple relation MLT = UT + 0.55 h for the data presented in this study. Two dispersive injection events, labeled as R1 (UT 1400–1800) and R2 (UT 1900–2200), were observed on the duskside and at premidnight, respectively, with a phase space density peak at higher energy occurring at earlier MLT. These dispersed injection events are due to energy-dependent westward magnetic gradient drift, where higher-energy protons, originating from an isolated injection event near midnight, arrive earlier at the spacecraft. As a consequence of this drift, the protons develop a ring distribution with peak energy near ~10 keV, decreasing at later MLT. These transient dispersive injected protons are eventually replaced by the semipermanent plasma sheet population (~keV) with no discernible ring structure (at UT 1800 for R1 and UT 2200 for R2). *Dst* remains above −35 nT throughout the day while large *AE* (>200 nT) is observed a few hours prior to R1 and R2, indicating that these proton rings are probably associated with impulsive substorm injections near midnight.

[16] To examine whether these rings are unstable to MS waves, the Alfven energy E_A (= $m_{H^+}V_A^2/2$) is superimposed by dots, with the black and white colors representing cold

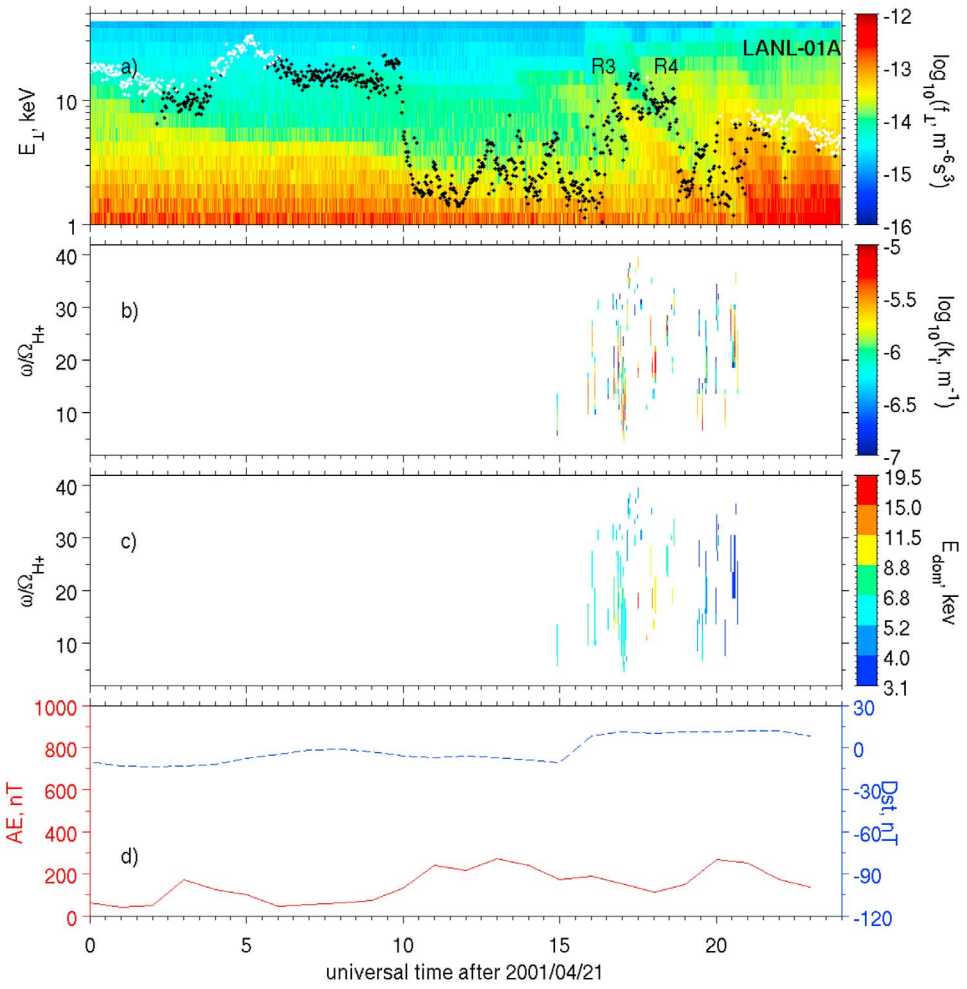

Figure 4. Same as Figure 3 but for 21 April 2001.

proton dominated plasma ($N_{lp} > N_{hp}$) and hot proton dominated plasma ($N_{lp} \leq N_{hp}$), respectively. Both observed rings occur in the region of cold plasma domination, with a ring energy E_R (= $m_{H^+}V_R^2/2$) comparable to the local Alfven energy (~10 keV), suggesting instability of MS waves. Using equation (3), the convective growth rate of magnetosonic waves at fixed wave normal angle (θ = 89.5°) is calculated for exact multiples of the proton gyrofrequency $\omega = m_\omega \Omega_{H^+}$, where m_ω is a whole number from 2 to 43. Figure 3b shows the frequencies and times at which the convective growth rate is positive. The observed proton rings during event R1 tend to excite MS waves over a broad frequency range, from a few Ω_{H^+} at local time (LT) 1500 where the ring energy ($E_R \approx$ 15 keV) is above Alfven energy (~10 keV), shifting upward to 35 Ω_{H^+} at LT 1700 when the ring energy falls below the Alfven energy by a factor of ~2. Calculated growth rates have a peak value on the order of 10^{-5} m^{-1}, which is 2 orders of magnitude greater than suggested by earlier estimates for MS wave instability [*Horne et al.*, 2000]. Two factors contribute to this difference. First, the peak proton ring phase space density (~10^{-13} m^{-6} s^3) observed here near the dusk sector at synchronous orbit is more than an order of magnitude larger than that reported ~5×10^{-15} m^{-6} s^3 at lower L (3.7 < L < 4.7) by *Horne et al.* [2000]. Secondly, the raw $f_\perp$ data, without smoothing or fitting, have been utilized here for calculation of the growth rate. The energy interval E_{dom} corresponding to the dominant contribution to the growth rate is shown in panel c. E_{dom} lies just below the proton ring energy, and gradually declines at later MLT. Unstable MS waves excited at higher frequency for later MLT are driven by the proton distribution with lower ring energy (Figure 1). Note that spurious growth, due to positive $df_\perp/dv_\perp$ associated with statistical fluctuations in the measured $f_\perp$ at lower energy (E_{dom} < a couple of keV) has been carefully removed, whenever E_{dom} is associated with these fluctuations rather than associated with a ring distribution. While positive $df_\perp/dv_\perp$ below the ring energy is responsible for exciting MS waves over the predicted frequency range, negative $df_\perp/dv_\perp$ above the ring energy and at lower energy (< a few keV) contributes to the damping, predominately for frequencies below and above the unstable frequency band, respectively (Figure 1). A similar frequency pattern of unstable MS waves occurs during event R2 except that energy of the proton rings is always below the local Alfven energy, resulting in unstable frequencies above ~20 Ω_{H^+}.

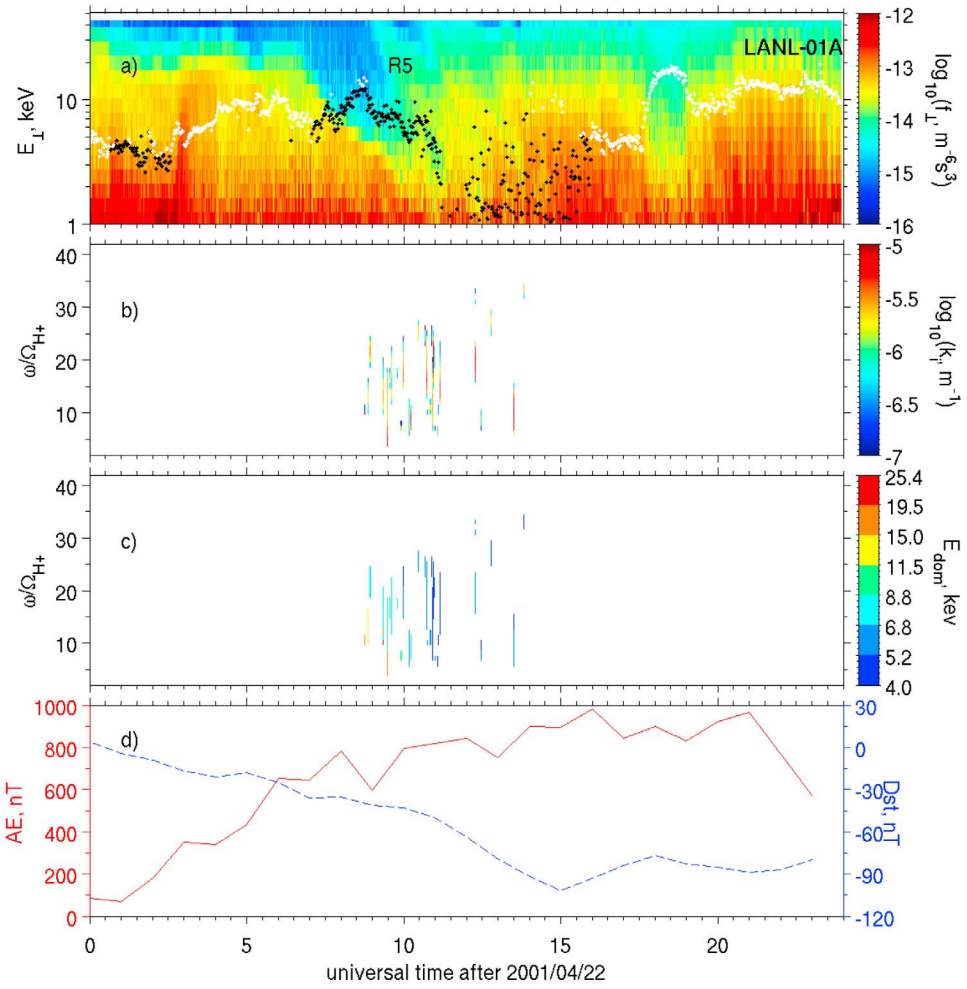

Figure 5. Same as Figure 3 but for 22 April 2001.

[17] Figure 4 shows MPA observations and the associated MS wave instability analysis for 21 April 2001. A high-density plasmaspheric plume (~10 cm^{-3}) occurs in the afternoon (UT 1000–1700) and in the evening sector (UT 1830–2100), accompanied by large variations in plasma density (and thus Alfven energy). The density variations appear to be associated with enhancement and variation in convection strength due to impulsive substorm activity (*AE* greater than 200 nT during each interval), which leads to drainage of plasmaspheric plasma toward the dayside. Dispersionless injection is observed in the energetic proton spectrum near midnight, while two pronounced dispersive injections (events R3 and R4) occur on the dusk side and in the premidnight sector, respectively. These two events overlap near dusk (UT 1700–1800) and occur during a period of highly variable plasma density. There is no evidence for ion rings at this satellite prior to 1500 UT. Furthermore, despite the development of a ring distribution in the high-density plume between 1500 and 1600 UT, the Alfven energy (~2 keV) is well below the ring energy (~10 keV), which stabilizes MS wave excitation over all proton harmonic gyrofrequencies due to strong damping contributed by the portion of $f_\perp$ at low energy (< 2 keV). The reduction in plasma density between 1630 and 1700 UT during event R3 causes the Alfven energy to increase and approach the observed ring energy, leading to instability over a broad range of wave frequencies from 4 to ~25 Ω_{H^+}. During event R4, the unstable frequency band is also modulated by the ratio E_R/E_A. Near 1730 UT, waves at low proton harmonics are excited at the leading edge of the event R4, with the frequency shifting toward higher proton harmonics (~30 Ω_{H^+}) near 1830 UT, as a result of the decrease in E_R at later MLT. The unstable frequency drops below 15 Ω_{H^+} inside the high-density plume near 1930 UT, due to a sudden decrease of E_A. Density fluctuations inside the plume near 1930–2100 UT cause the frequency range of unstable MS waves to vary in an unsystematic way.

[18] The main phase of the geomagnetic storm occurred on 22 April 2001, shown in Figure 5, with *Dst* falling to −100 nT and *AE* increasing to ~1000 nT near 1500 UT. Multiple dispersionless injection events occur throughout the nightside (1900 UT on 21 April to 0400 UT on 22 April). Several overlapping dispersive injection events, occurring less than approximately a couple of hours apart, are observed near noon and over the afternoon sector. The only pronounced dispersive proton injection (event R5) was observed near noon in the low-density region on the westward side of a plume with fine-scale density variation that

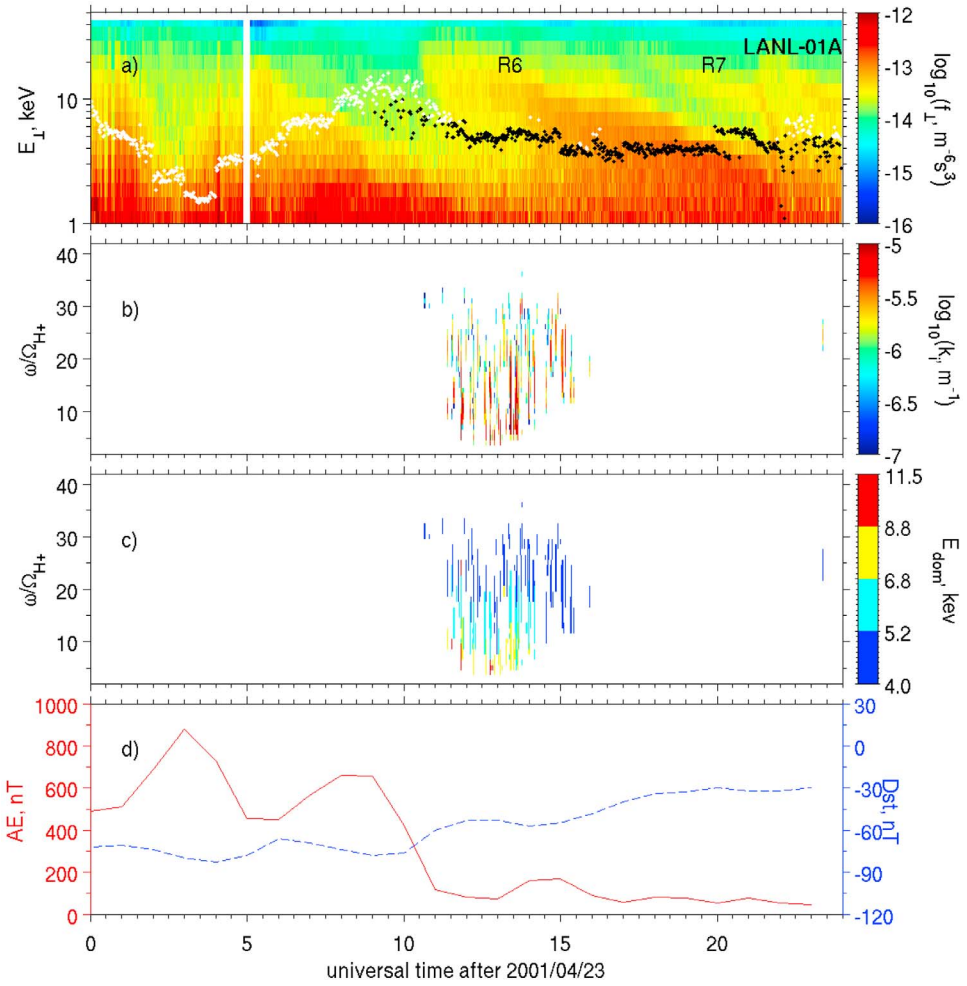

Figure 6. Same as Figure 3 but for 23 April 2001.

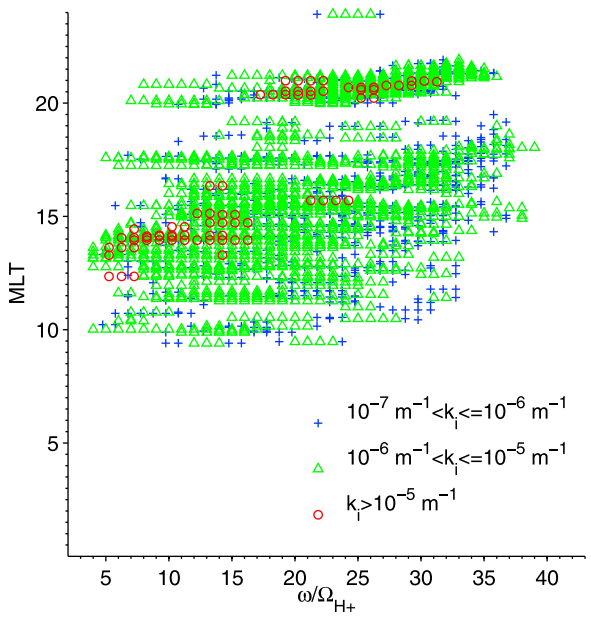

Figure 7. Scatterplot of MLT regions where convective growth rate of magnetosonic waves is greater than 10^{-7} m^{-1} versus wave frequency normalized to local proton gyrofrequency ω/Ω_{H+}, based on our instability analysis over the 4 day period from 20 April 2001 to 23 April 2001. Different symbols represent the different levels of the growth rate: blue pluses for 10^{-7} m^{-1} < $k_i \leq 10^{-6}$ m^{-1}, green triangles for 10^{-6} m^{-1} < $k_i \leq 10^{-5}$ m^{-1}, and red circles for $k_i > 10^{-5}$ m^{-1}.

forms from noon to dusk. The high Alfven energy (~6 keV) outside the plume near UT 0900–1000 reduces the damping contribution from the low-energy component (< 3 keV). The high ratio of proton ring energy to Alfven energy during this interval favors the excitation of MS waves at low proton harmonic gyrofrequencies (3–20 Ω_{H^+}). As the Alfven energy falls to ~3 keV, the contribution from damping becomes sufficient to suppress MS waves over all proton harmonic gyrofrequencies between 1130–1200 UT.

[19] Two pronounced dispersive proton injection events (R6 and R7) occur during the recovery phase of the geomagnetic storm on 23 April 2001, shown in Figure 6. Event R6, which occurs in the afternoon sector, appears to be associated with pronounced substorm activity prior to 0800 UT. The strong proton ring distribution during R6 is unstable to MS wave excitation over a broad frequency spectrum from a few Ω_{H^+} to 30 Ω_{H^+}. The weaker event R7 might be associated with a smaller *AE* enhancement (~200 nT) a few hours prior to the injection. However, during the event R7, the ring energy is well above the Alfven energy. As a consequence this event is stable to the excitation of magnetosonic waves at all wave frequencies due to damping by the low-energy component.

[20] Table 1 gives a summary of the number of PSDs measured by the MPA instrument for the chosen 4 day period. 1639 out of total 3790 PSD measurements are chosen for instability analysis, and 394 of them are found to be unstable for MS waves (with peak growth rate among varying proton harmonic frequencies exceeding 10^{-7} m^{-1}). For 304 PSD measurements, the peak growth rate exceeds 10^{-6} m^{-1}. Figure 7 shows a scatterplot of MLT range where the calculated MS wave growth rate exceeds 10^{-7} m^{-1}, against wave frequencies normalized to local proton gyro frequency, with three categories based on the levels of the calculated growth rate: 10^{-7} m^{-1} < $k_i \leq 10^{-6}$ m^{-1} (blue pluses), 10^{-6} m^{-1} < $k_i \leq 10^{-5}$ m^{-1} (green triangles) and $k_i > 10^{-5}$ m^{-1} (red circles). The majority (67%) of calculated growth rates fall in the range from 10^{-6} m^{-1} to 10^{-5} m^{-1}, while 30% are in the range from 10^{-7} m^{-1} to 10^{-6} m^{-1}, and only 3% have the growth rate larger than 10^{-5} m^{-1} with largest value ~2 × 10^{-5} m^{-1}. MS wave instability at geosynchronous orbit occurs over a broad range of wave frequency from ~5 to 35 Ω_{H^+} and over a broad MLT range from 1000 to 2200, where the proton ring distributions are preferentially observed. No proton ring distribution is seen in the dawn sector during the chosen time period. This MLT distribution of unstable magnetosonic waves is consistent with the previous statistical results of *Perraut et al.* [1982, Figure 10a], showing large probability (> 30%) of magnetosonic wave events detected in the MLT range from 1100 to 0200 and few events detected in the dawn sector.

4. Conclusion and Discussion

[21] Proton phase space density at 90° pitch angle measured by MPA on board a LANL geosynchronous orbiting satellite during the 2001 April storm has been analyzed, to examine the potential instability of magnetosonic waves. Our principal conclusions are summarized as follows:

[22] 1. Proton rings associated with dispersive injection events develop over a broad spatial region between noon and premidnight. They appear to be associated with individual substorm injections on the nightside during non storm time periods. During the magnetic storm main phase, multiple injections on the nightside tend to merge together, with pronounced proton rings only apparent at the leading edge of the injection. This behavior of the ion rings observed at $L \approx 6.6$ during the storm main phase appears to

Table 1. The Number of Proton Phase Density Measured by the MPA Instrument on the LANL-01A Spacecraft

Date	Total Number	Number Selected for Instability Analysis[a]	Number Found to Be Unstable[b]
20 Apr 2001	803	325 (14 ≤ UT ≤ 22)	177 (144)
21 Apr 2001	999	417 (14 ≤ UT ≤ 24)	68 (43)
22 Apr 2001	997	314 (8.5 ≤ UT ≤ 16)	41 (28)
23 Apr 2001	991	583 (10 ≤ UT ≤ 24)	108 (89)
All 4 days	3790	1639	394 (304)

[a]Universal time range (in unit of h) selected for instability analysis is given in parentheses.
[b]The number of ion phase space density found to be unstable and with peak growth rate greater than 10^{-6} m^{-1} is given in parentheses.

be different from the RAM simulation results at lower L reported by *Chen et al.* [2010b]. In that simulation the proton ring distributions arose as a consequence of quasi-steady injection into the ring current driven by a global convection electric field. The simulation did not include any localized substorm processes. The present observational results suggest that the electric field used in global ring current modeling needs to be modified to accommodate the substorm injection process in order to better simulate the development of the ion ring distribution observed at geosynchronous orbits on the duskside during times of significant substorm activity.

[23] 2. The observed proton rings provide a source of free energy for magnetosonic wave instability over a broad frequency range from several to 35 Ω_{H^+}, depending on the ratio of ring velocity to Alfven velocity. Higher (or lower) values of V_R/V_A tend to excite MS waves at lower (or higher) proton harmonics. Instability is favored when the Alfven energy is comparable to the energy of proton ring and sufficiently higher than the low-energy (~keV) component, which causes wave damping.

[24] The calculated local convective growth rates indicate the dominant source region of MS wave excitation during the April 2001 storm. However, the ability of MS waves to propagate both radially and azimuthally, which could lead to mixing of wave power from a broad source region nearby, should produce a broader frequency spectrum than indicated by these local calculations. Three-dimensional ray tracing will be required to obtain the path-integrated gain. This is beyond the scope of the present paper, but will be investigated in the future.

[25] Although no wave measurement is presented in this study, we do intend to test our theoretical instability analysis in a simultaneous observation of ion distribution and magnetosonic wave emission on satellites such as CRRES, THEMIS and Cluster. Such direct comparison will complement the present study. We also plan to extend our present analysis and perform a statistical study to investigate the global characteristics of the proton ring development at geostationary orbit, using measurement from MPA detectors on board multiple LANL geosynchronous orbiting satellites.

[26] **Acknowledgments.** The research was supported by NASA grants NNX08AQ88G, NNH08AJ01I, and NNX08A135G. Work at Los Alamos was conducted under the auspices of the U.S. Department of Energy. The authors thank SPDF OMNIWeb Plus service for providing the *Dst* and hAE indices, solar wind dynamic pressure, and *Y* and *Z* components of the interplanetary magnetic field.

[27] Robert Lysak thanks the reviewers for their assistance in evaluating this paper.

References

Bame, S. J., D. J. McComas, M. F. Thomsen, B. L. Barraclough, R. C. Elphic, J. P. Glore, J. T. Gosling, J. C. Chavez, E. P. Evans, and F. J. Wymer (1993), Magnetospheric plasma analyzer for spacecraft with constrained resources, *Rev. Sci. Instrum.*, *64*, 1026–1033, doi:10.1063/1.1144173.

Blum, L. W., E. A. MacDonald, S. P. Gary, M. F. Thomsen, and H. E. Spence (2009), Ion observations from geosynchronous orbit as a proxy for ion cyclotron wave growth during storm times, *J. Geophys. Res.*, *114*, A10214, doi:10.1029/2009JA014396.

Boardsen, S. A., D. L. Gallagher, D. A. Gurnett, W. K. Peterson, and J. L. Green (1992), Funnel-shaped, low-frequency equatorial waves, *J. Geophys. Res.*, *97*, 14,967–14,976, doi:10.1029/92JA00827.

Bortnik, J., and R. M. Thorne (2010), Transit time scattering of energetic electrons due to equatorially confined magnetosonic waves, *J. Geophys. Res.*, *115*, A07213, doi:10.1029/2010JA015283.

Chen, L., R. M. Thorne, V. K. Jordanova, C. Wang, M. Gkioulidou, L. Lyons, and R. B. Horne (2010a), Global simulation of EMIC wave excitation during the 21 April 2001 storm from coupled RCM-RAM-HOTRAY modeling, *J. Geophys. Res.*, *115*, A07209, doi:10.1029/2009JA015075.

Chen, L., R. M. Thorne, V. K. Jordanova, and R. B. Horne (2010b), Global simulation of magnetosonic waves instability in the storm time magnetosphere, *J. Geophys. Res.*, *115*, A11222, doi:10.1029/2010JA015707.

Curtis, S. A., and C. S. Wu (1979), Gyroharmonic emissions induced by energetic ions in the equatorial plasmasphere, *J. Geophys. Res.*, *84*, 2597–2607, doi:10.1029/JA084iA06p02597.

Denton, R. E., M. F. Thomsen, K. Takahashi, R. R. Anderson, and H. J. Singer (2011), Solar cycle dependence of bulk ion composition at geosynchronous orbit, *J. Geophys. Res.*, doi:10.1029/2010JA016027, in press.

Gary, S. P., K. Liu, D. Winske, and R. E. Denton (2010), Ion Bernstein instability in the terrestrial magnetosphere: Liner dispersion theory, *J. Geophys. Res.*, *115*, A12209, doi:10.1029/2010JA015965.

Gurnett, D. A. (1976), Plasma wave interactions with energetic ions near the magnetic equator, *J. Geophys. Res.*, *81*, 2765–2770, doi:10.1029/JA081i016p02765.

Horne, R. B., G. V. Wheeler, and H. S. C. K. Alleyne (2000), Proton and electron heating by radially propagating fast magnetosonic waves, *J. Geophys. Res.*, *105*, 27,597–27,610, doi:10.1029/2000JA000018.

Horne, R. B., R. M. Thorne, S. A. Glauert, J. M. Albert, N. P. Meredith, and R. R. Anderson (2005), Timescale for radiation belt electron acceleration by whistler mode chorus waves, *J. Geophys. Res.*, *110*, A03225, doi:10.1029/2004JA010811.

Horne, R. B., R. M. Thorne, S. A. Glauert, N. P. Meredith, D. Pokhotelov, and O. Santolík (2007), Electron acceleration in the Van Allen radiation belts by fast magnetosonic waves, *Geophys. Res. Lett.*, *34*, L17107, doi:10.1029/2007GL030267.

Jordanova, V. K., R. M. Thorne, W. Li, and Y. Miashi (2010), Excitation of whistler-mode chorus from global ring current simulations, *J. Geophys. Res.*, *115*, A00F10, doi:10.1029/2009JA014810.

Kasahara, Y., H. Kenmochi, and I. Kimura (1994), Propagation characteristics of the ELF emissions observed by the satellite Akebono in the magnetic equatorial region, *Radio Sci.*, *29*, 751–767, doi:10.1029/94RS00445.

Li, W., Y. Y. Shprits, and R. M. Thorne (2007), Dynamic evolution of energetic outer zone electrons due to wave-particle interactions during storms, *J. Geophys. Res.*, *112*, A10220, doi:10.1029/2007JA012368.

MacDonald, E. A., M. H. Denton, M. F. Thomsen, and S. P. Gary (2008), Superposed epoch analysis of a whistler instability criterion at geosynchronous orbit during geomagnetic storms, *J. Atmos. Sol. Terr. Phys.*, *70*, 1789–1796, doi:10.1016/j.jastp.2008.03.021.

Meredith, N. P., R. B. Horne, and R. R. Anderson (2008), Survey of magnetosonic waves and proton ring distributions in the Earth's inner magnetosphere, *J. Geophys. Res.*, *113*, A06213, doi:10.1029/2007JA012975.

Němec, F., O. Santolík, K. Gereová, E. Macúšová, Y. de Conchy, and N. Cornilleau-Wehrlin (2005), Initial results of a survey of equatorial noise emissions observed by the Cluster spacecraft, *Planet. Space Sci.*, *53*, 291–298, doi:10.1016/j.pss.2004.09.055.

Olsen, R. C., S. D. Shawhan, D. L. Gallagher, C. R. Chappell, and J. L. Green (1987), Plasma observations at the Earth's magnetic equator, *J. Geophys. Res.*, *92*, 2385–2407, doi:10.1029/JA092iA03p02385.

Perraut, S., A. Roux, P. Robert, R. Gendrin, J. Sauvaud, J. Bosqued, G. Kremser, and A. Korth (1982), A systematic study of ULF waves above F_{H+} from GEOS 1 and 2 measurements and their relationships with proton ring distributions, *J. Geophys. Res.*, *87*, 6219–6236, doi:10.1029/JA087iA08p06219.

Roberts, W. T., Jr., J. L. Horwitz, R. H. Comfort, C. R. Chappell, J. H. Waite Jr., and J. L. Green (1987), Heavy ion density enhancements in the outer plasmasphere, *J. Geophys. Res.*, *92*, 13,499–13,512, doi:10.1029/JA092iA12p13499.

Russell, C. T., R. E. Holzer, and E. J. Smith (1970), OGO 3 observations of ELF noise in the magnetosphere: 2. The nature of the equatorial noise, *J. Geophys. Res.*, *75*, 755–768, doi:10.1029/JA075i004p00755.

Santolík, O., J. S. Pickett, D. A. Gurnett, M. Maksimovic, and N. Cornilleau-Wehrlin (2002), Spatiotemporal variability and propagation of equatorial noise observed by Cluster, *J. Geophys. Res.*, *107*(A12), 1495, doi:10.1029/2001JA009159.

Thomsen, M. F., D. J. McComas, G. D. Reeves, and L. A. Weiss (1996), An observational test of the Tsyganenko (T89a) model of the magneto-

spheric field, *J. Geophys. Res.*, *101*, 24,827–24,836, doi:10.1029/96JA02318.

Tsyganenko, N. A. (1995), Modeling the Earth's magnetospheric magnetic field confined within a realistic magnetopause, *J. Geophys. Res.*, *100*, 5599–5612, doi:10.1029/94JA03193.

Tsyganenko, N. A. (1996), Effects of the solar wind conditions in the global magnetospheric configurations as deduced from data-based field models, in *International Conference on Substorms*, edited by E. J. Rolfe and B. Kaldeich, *Eur. Space Agency Spec. Publ.*, *389*, 181.

Young, D. T., H. Balsiger, and J. Geiss (1982), Correlations of magnetospheric ion composition with geomagnetic and solar activity, *J. Geophys. Res.*, *87*, 9077–9096, doi:10.1029/JA087iA11p09077.

L. Chen and R. M. Thorne, Department of Atmospheric Sciences, University of California, Los Angeles, CA 90024, USA. (clj@atmos.ucla.edu)

R. B. Horne, British Antarctic Survey, Natural Environment Research Council, Cambridge CB3 0ET, UK.

V. K. Jordanova and M. F. Thomsen, Los Alamos National Laboratory, Los Alamos, NM 87545, USA.